Multi-wavelength aerosol LIDAR signal pre-processing: practical considerations

A Rodríguez-Gómez[1], F Rocadenbosch[1], M Sicard[1], D Lange[2], R Barragán[1], O Batet[3], A Comerón[1], M A López Márquez[1], C Muñoz-Porcar[1], J Tiana[1] and S Tomás[4]

[1]Barcelona Lidar Station, Remote Sensing Laboratory (RSLAB), Department of Signal Theory and Communications, BarcelonaTech University (UPC), Spain.
[2]Departamento de Ciencias Exactas e Ingeniería, Universidad Católica Boliviana San Pablo, Bolivia
[3]Expert Ymaging S.L., IC3 - Catalan Institute of Climate Sciences
[4]Instituto de Ciencias del Espacio, CSIC, Spain.

E-mail: alejandro@tsc.upc.edu

Abstract. Elastic lidars provide range-resolved information about the aerosol content in the atmosphere. Nevertheless, a number of pre-processing techniques need to be used before performing the inversion of the detected signal: range-correction, time-averaging, photon-counting channel dead-time correction, overlap correction, Rayleigh-fitting and gluing of both channels.

1. Introduction

Elastic lidars provide range-resolved information about the aerosol content in the atmosphere [1]. Before performing the signal inversion, that will provide this information, a number of pre-processing techniques need to be performed. This paper provides a practical approach to some of them.

2. Range-correction and time-averaging

Figure 1 shows the system description of UPC 6-channel elastic lidar [2]. It includes a Nd:YAG laser transmitter with second and third harmonic generators, that produces pulses at 1064 nm, 532 nm and 355 nm. The receiving system includes a 36-cm telescope, a polychromator unit and six receiving channels: 1064, 607, 532, 407, 387 and 355 nm; in every channel both power (analogic) and photon counting reception is performed. For the rest of this paper we will be dealing with the received signal at 532 nm.

Figure 2 shows the received signal for a one-pulse transmitted signal. Different features must be pointed out: most of the signal is negligible, apart from a non-zero offset in the analog channel. According to the lidar equation [1]:

$$P(R) = \frac{E_{pulse} A_{teles} c}{2R^2} \left[\beta(R)\right] \cdot e^{-2\int_0^R [\alpha(x)]dx} \quad (1).$$

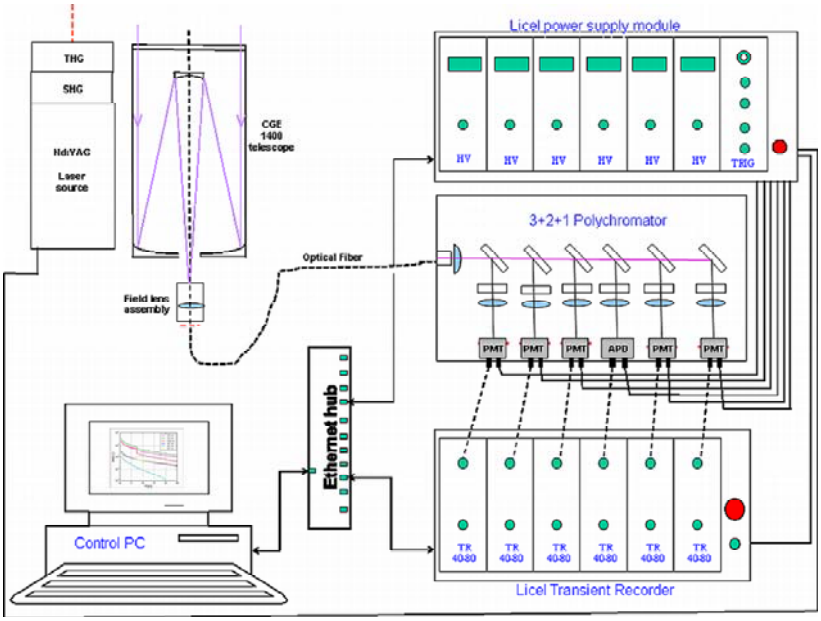

Figure 1. UPC elastic lidar system general layout [2].

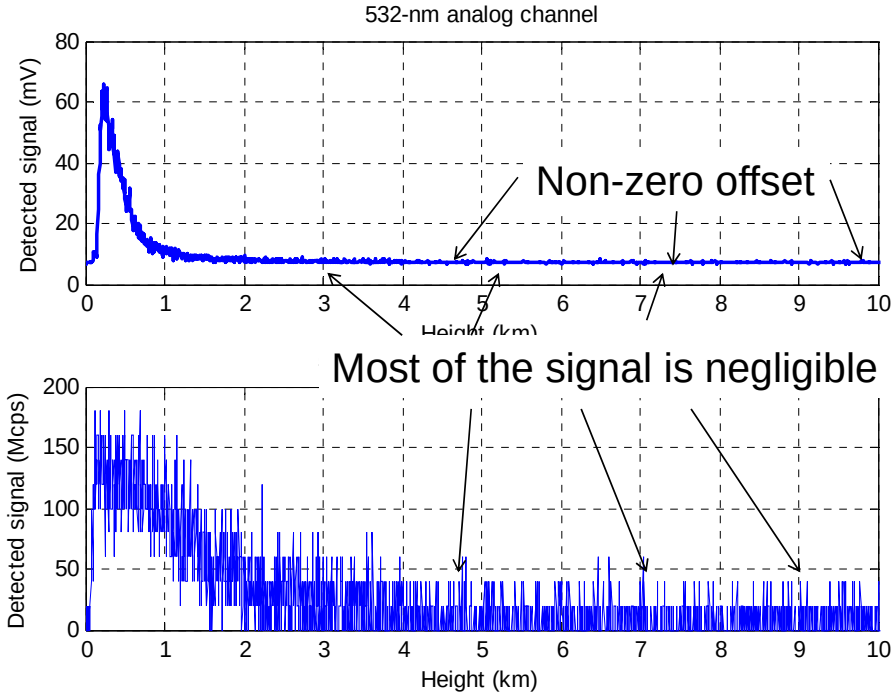

Figure 2. Received signal for one-pulse transmitted.

The received signal power ($P(R)$) contains information about the atmospheric back-scattering ($\beta(R)$) and extinction ($\alpha(R)$). It also states that the received signal is inversely proportional to the squared distance. The rest of the parameters are: E_{pulse}, the transmitter laser pulse energy and A_{teles}, the collecting area of the receiving telescope. In order to obtain a useful signal we will apply offset subtracting, 150-minute averaging and range correction (multiplying the signal times the squared distance). This measurement is one of the regular measurements which our group performs simultaneously with close passes of CALIPSO satellite [3].The result of the previous processes can be seen in Figure 3.

3. Dead-time correction

From the previous section, it must be pointed out that both (analog and photon-counting) channels present low signal levels at short distance. In the photon-counting channel, dead-time effect (an event will not be recorded when the time interval between its occurrence and the occurrence of the last recorded event is smaller than some given interval, τ_{dead}) must be corrected. A good estimate of the true number of the collected photons can be obtained with the equation [2]:

$$N_{real} = \frac{N_{meas}}{1 - \tau_{dead} N_{meas}} \quad (2)$$

The result of applying this relation is plotted in Figure 4.

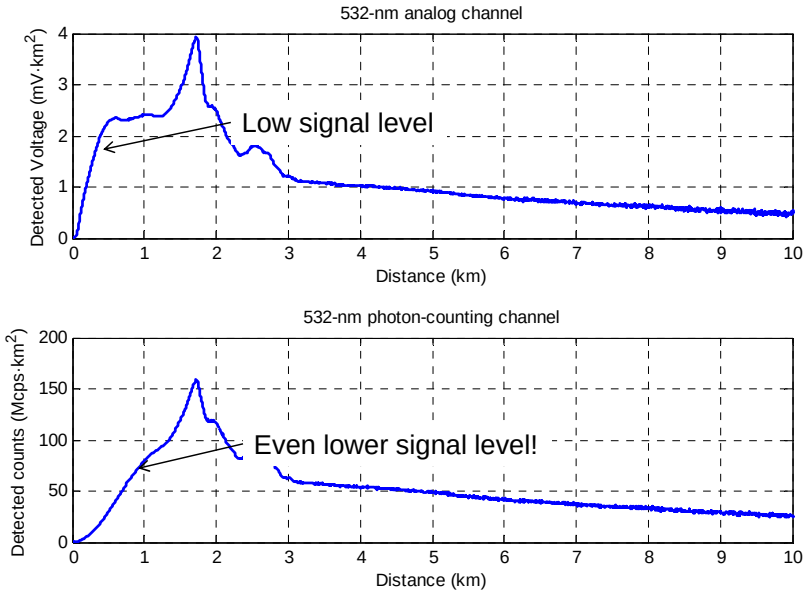

Figure 3. Time-averaged and ranged corrected signals.

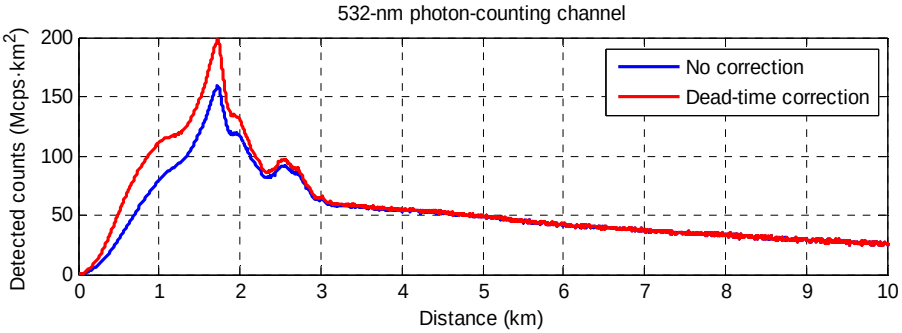

Figure 4. Dead-time correction.

4. Overlap correction

Even though it is not indicated in Figure 1, there usually is a non-negligible distance between the transmitter and the receiving telescope axes. There could also be some kind of misalignment between both axes. The effect of this separation is wonderfully explained in [1]. Figure 5 shows the effect of the separation of both axes, together with the actual values of laser beam divergence and receiver field of view.

For these values, the effect of the incomplete overlap can be either computed theoretically or estimated from measurements. Wandinger and Ansmann [5] demonstrated that the effect of the overlap in a particular measurement can be obtained by comparing the KFS inversion (affected by the overlap effect) and the Raman inversion (not affected). The result of the comparison (which involves techniques out the scope of this paper) is shown in Figure 6. Overlap is computed from 100 to 1000 m. Then it can be applied to correct both analog and photon-counting channels. The effect of this correction is plotted in Figure 7. It must be noted that, as expected, the result with the analog channel is a stronger return from low altitudes, where the concentration of aerosols is usually highest. Nevertheless, the low panel shows still low values for the photon-counting channel: these low values are usually attributed to saturation of the event counter when many photons are available. This saturation cannot be corrected reliably. Thus, some combination between the analog and the photon-counting signals must be performed, as it will be described in Section 6.

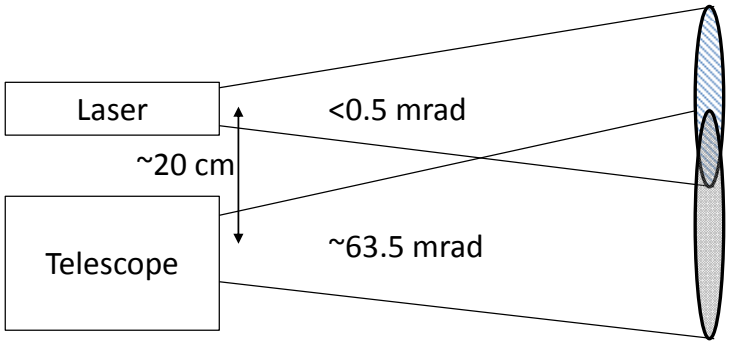

Figure 5. Illustration of the effect of partial overlap between the transmitted beam and the receiver field of view (adapted from [1]) .

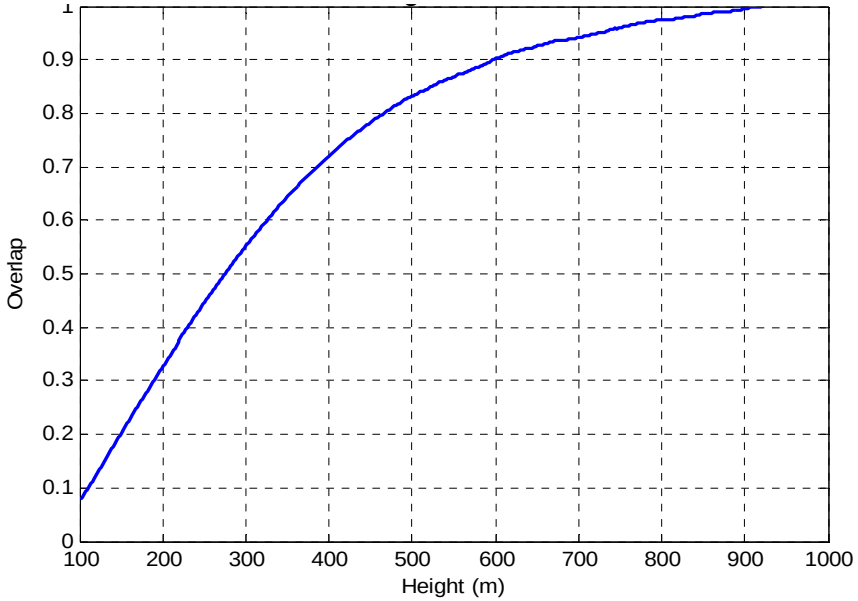

Figure 6. Estimation of overlap between the area illuminated by the laser and that seen by the lidar receiver.

5. Rayleigh fit

In all the plots shown before, it can be seen that neither the analog nor the photon-counting signals reach a zero-value, which is not consistent with the fact that aerosols are found only in the first kilometres of the troposphere. To get an answer to this fact, one has to remember that two light-

scattering mechanisms are present in the atmosphere: Mie scattering, produced by aerosols (roughly of the same size as the light wavelength) and Rayleigh scattering, produced by atmospheric constituent gases. With this in mind, we should rewrite equation (1) in the form:

$$P(R) = \frac{E_{pulse} A_{telescope} c}{2R^2} \left[\beta_{aer}(R) + \beta_{gases}(R) \right] \cdot e^{-2\int_0^R \left[\alpha_{aer}(x) + \alpha_{gases}(x) \right] dx} \quad (3)$$

So, the next step in the lidar signal pre-processing will be to identify the component produced by atmospheric gases in our signal and subtract it from the detected signal. The gas component can be either computed from standard atmospheric models [6] or from measurements obtained by "radio-sounds".

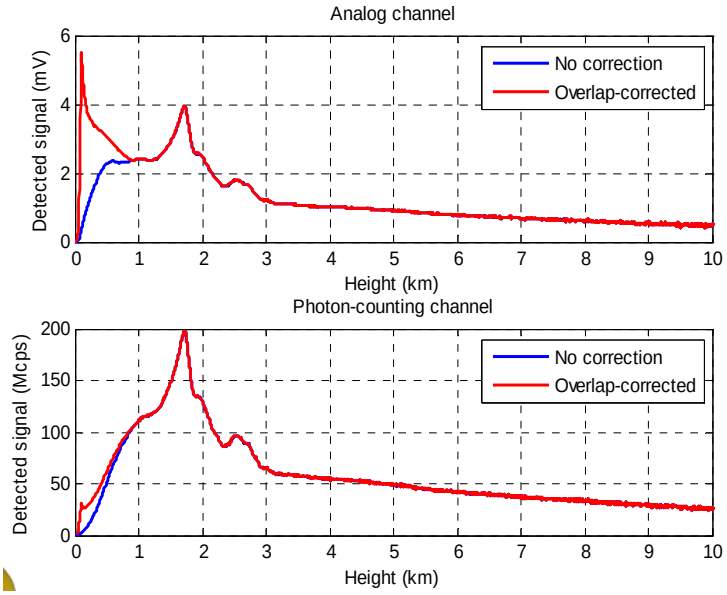

Figure 7. Effect of overlap correction.

Radio-sound measurements are performed in Barcelona by the Catalan Meteorological Service twice a day, at 00:20 and 12:20 UTC. So the lidar systems can be fitted by using a least squared error approach in the range of height values where no aerosol is expected. Figure 8 shows both the Rayleigh profiles computed from radio-sound measurements and the lidar signals fitted to the Rayleigh profile in the height interval between 6 and 10 km.

6. Gluing

Along the different plots presented in this paper, the analog channel represents more accurately the aerosol return at low altitude. Although it might not be evident, the photon-counting channel provides better Signal-to-Noise ratio at high altitude. For this reason, the two signals are combined in a process called gluing. Several strategies have been proposed [4] but we follow that proposed by Diego Lange in his PhD dissertation [7]. The result is presented in Figure 9.

7. Aerosol-only return

Finally, the signal due only to aerosol return can be identified and fed to the inversion algorithms, by subtracting the gas return (green line in Figure 9) from the composed signal (blue line in Figure 9). The result is plotted in Figure 10.

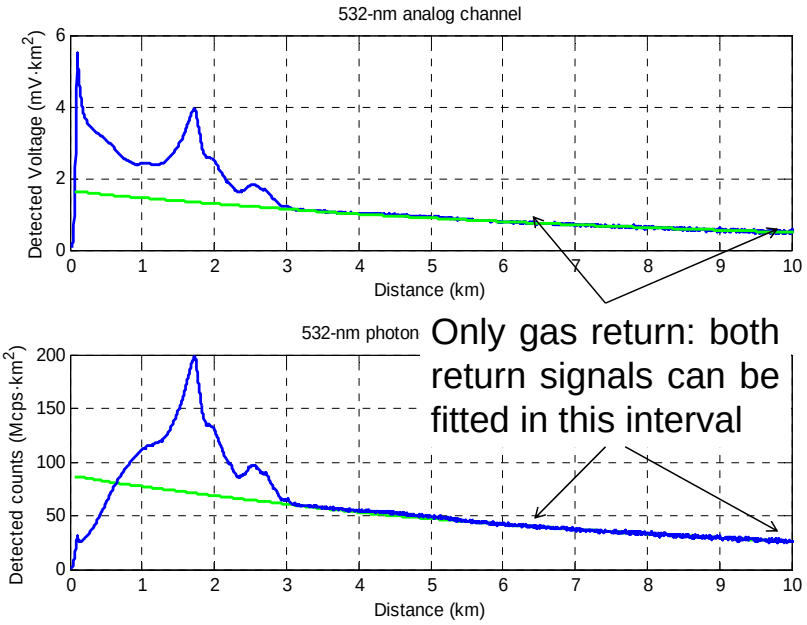

Figure 8. Rayleigh profiles and Rayleigh-fitted signals from 6 to 10 km.

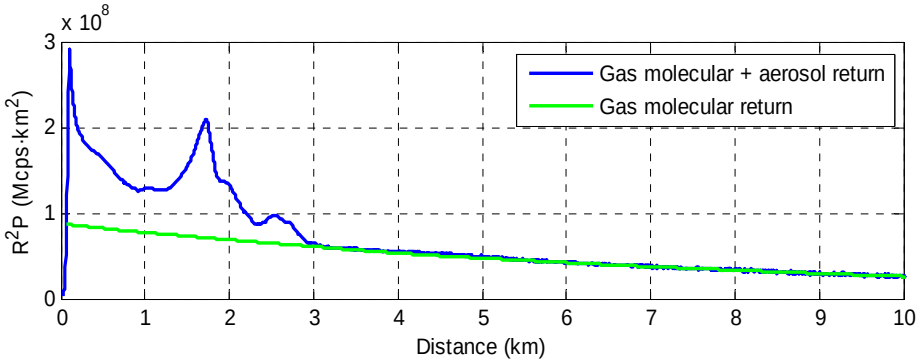

Figure 9. Resulting signal from gluing analog and photon-counting channels.

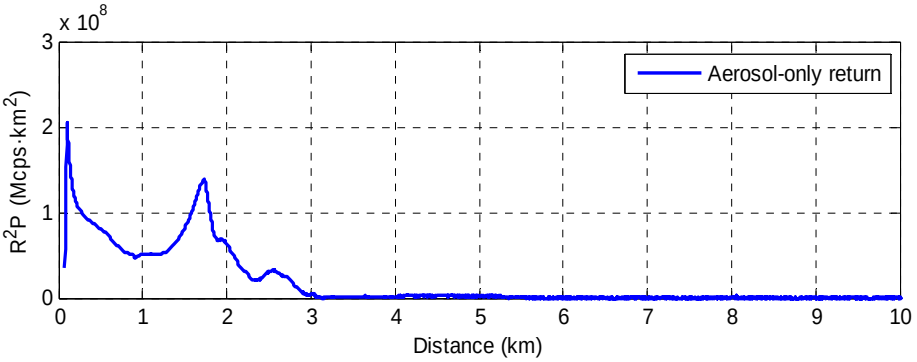

Figure 10. Aerosol-only return signal.

Acknowledgements
This work has been financed by Spanish Ministry for Economy and Competitiveness, through projects TEC2012-34799 and TEC2012-34575.

References

[1] Measures R, Laser Remote Sensing: Fundamentals and Applications, Krieger Publishing Company 1992
[2] Kumar D, Rocadenbosch F, Concept Design, Analysis, and Integration of the New UPC Multispectral Lidar System, UPC 2012
[3] http://www-calipso.larc.nasa.gov/about/payload.php
[4] Licel GmbH, Licel Ethernet Controller – Installation and Reference Manual.
[5] Wandinger U, Ansmann A, "Experimental determination of the lidar overlap profile with Raman lidar," *Appl. Opt*. 41, 511-514 (2002).
[6] http://www.atmosculator.com/The%20Standard%20Atmosphere.html
[7] Lange D, Rocadenbosch F, Lidar and S-band radar profiling of the atmosphere: Adaptive processing for Boundary-Layer monitoring, optical-parameter error estimation, and application cases, Universitat Politècnica de Catalunya-BarcelonaTech, 2014.